Convergence Characteristics of the Crank-Nicolson-Galerkin Scheme for Linear Parabolic Systems

Jin-Rae Cho*, Dae-Yul Ha, Tae-Jong Kim
Research Institute of Mechanical Technology, Pusan National University, Jangjeon-Dong, Kumjung-Ku, Pusan 609-735, Korea

This paper is concerned with the investigation on the stability and convergence characteristics of the Crank-Nicolson-Galerkin scheme that is widely being employed for the numerical approximation of parabolic-type partial differential equations. Here, we present the theoretical analysis on its consistency and convergence, and we carry out the numerical experiments to examine the effect of the time-step size Δt on the h- and p-convergence rates for various mesh sizes h and approximation orders p. We observed that the optimal convergence rates are achieved only when Δt, h and p are chosen such that the total error is not affected by the oscillation behavior. In such case, Δt is in linear relation with DOF, and furthermore its size depends on the singularity intensity of problems.

Key Words : Crank-Nicolson-Galerkin Scheme, Convection-Type Problem, Stability and Consistency, Mesh Parameters, Optimal Convergence Rate

1. Introduction

For the numerical approximation of the parabolic-type partial differential equations, the Crank-Nicolson-Galerkin scheme has been widely employed thanks to its higher time discretization accuracy compared to other first-order schemes (Bieniasz et al., 1997 ; Cho et al., 2000 ; Tsukerman 1995). Even though this scheme is unconditionally convergent, it may suffer the inherent oscillation phenomenon unless the time-step size is insufficiently small to satisfy a specific time-space partitioning criterion depending on numerical data of the problem at hand.

The basic stability analysis of the Crank-Nicolson-Galerkin scheme has been laid down, and the theoretical argument on the critical time-step size securing non-oscillation results may refer to Johnson (1987) and Burnett (1988). However, the derived criterion for the critical time-step size does not secure h- and p-convergence rates, in most cases, because it is simply turned to prevent the oscillation by the largest eigenmode. Regarding to the temporal-spatial error estimate, Johnson (1987) established the fundamental mathematical framework for first-order schemes in his book. Nevertheless, the stability and convergence analysis of the Crank-Nicolson-Galerkin scheme is still focused by many researchers in a variety of engineering fields (Comini and Manzan 1994 ; Morjaria and Mukherjee 1981 ; Suresh et al., 1994). The reason is because the suitable time-step size is problem-dependent and the convergence-level parametric characteristics have not been sufficiently investigated.

We in this paper intend to investigate the stability and convergence characteristics of the Crank-Nicolson-Galerkin scheme with respect to the time-step size and the mesh parameters. For this goal, we first derive a priori temporal-spatial error estimate for convection-type problems, and then we carry out the parametric numerical experiments to the combination of three parameters Δt, h and p. From the numerical results, we

* Corresponding Author,
E-mail : jrcho@hywon.pusan.ac.kr
TEL : +82-51-510-2467; **FAX** : +82-51-514-7640
Research Institute of Mechanical Technology, Pusan National University, Pusan 609-735, Korea. (Manuscript **Received** October 6, 2001; **Revised** June 26, 2002)

Copyright (C) 2003 NuriMedia Co., Ltd.

examine the influence of the parameters on the h- and p-convergence rates of the scheme.

2. Convection-Type Problems

Figure 1 depicts a general convection-type heat transfer problem. The time-dependent temperature field $T(x;t)$ is governed by heat-diffusion equation based on Fourier's law, and the initial and boundary conditions:

$$\left.\begin{aligned} \rho c\frac{\partial T}{\partial t}-\Delta\cdot(\kappa\nabla T)=\frac{\partial q}{\partial t},\ \text{in } \Omega,\ t\in(0,\ t^*] \\ T(x)=T_0,\ \text{at } t=0 \\ T(x)=f(x;t),\ \text{on } \Gamma_D \\ -\kappa\nabla T\cdot n=h_c[T^s(x;t)-T_\infty],\ \text{on } \Gamma_N \end{aligned}\right\} \quad (1)$$

Here, c, κ and h_c indicate respectively the specific heat, the thermal conductivity and the heat convection coefficient, while $q\in L^2(\Omega)$ and t^* denote the internal heat source and the time interval under consideration. Furthermore, T^s and T_∞ denote the surface temperature on Γ_D and the constant surrounding temperature, respectively. A varying temperature $f(x;t)\in L^2(\Gamma_D)$ is applied to the essential boundary Γ_D, and the heat convection between the natural boundary Γ_N and the surrounding is allowed.

2.1 Temporal discretization and spatial formulation

Let us partition time period $[0,\ t^*]$ into uniform N sub-periods, then we have uniform time intervals $\Delta t=t^*/N$ and $(N+1)$ time stages $t_n=n\Delta t$, $(n=0,\ 1,\ \cdots,\ N)$. According to the Crank-Nicolson scheme, we have a sequence of semi-discrete converted boundary value problems for N time stages t_n, $(n=0,\ 1,\ 2,\ \cdots,\ N-1)$:

$$\left.\begin{aligned} \frac{\rho c}{\Delta t}(T_{n+1}-T_n)-\nabla\left\{\kappa\nabla\left(\frac{T_{n+1}+T_n}{2}\right)\right\}=\left(\frac{\partial q}{\partial t}\right)_{n+1/2},\ \text{in } \Omega \\ T_{n+1/2}=f_{n+1/2},\ \text{on } \Gamma_D \\ (-\kappa\nabla T\cdot n)_{n+1/2}=h_c(T^s_{n+1/2}-T_\infty),\ \text{on } \Gamma_N \end{aligned}\right\} \quad (2)$$

The converted boundary value problem (2) successively characterizes the temperature distribution $T(x;t_{n+1})$ at time stage t_{n+1} with the previously obtained solution $T(x;t_n)$ and the boundary data specified on Γ_D and Γ_N.

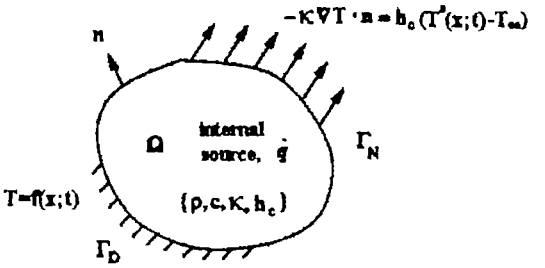

Fig. 1 A general two-dimensional heat convection problem

Now, we establish a weighted residual variational formulation for the solution $T(x;t_{n+1})$. We first define the space $V(\Omega)$ of admissible test temperature fields such that every function Ξ in $V(\Omega)$ has finite thermal strains and its trace on Γ_D vanishes:

$$V(\Omega)=\{\Xi(x):\Xi(x)\in H^1(\Omega),\ \gamma_D\Xi=0\} \quad (3)$$

with γ_D defined as a trace operator, $\gamma_D: H^1(\Omega)\rightarrow H^{1/2}(\Gamma_D)$. On the other hand, the trial function space $\tilde{V}_{n+1}(\Omega)$ for time stage t_{n+1} is defined as a linear manifold of $V(\Omega)$

$$\tilde{V}_{n+1}(\Omega)=V(\Omega)+\{w^*\}_{n+1} \quad (4)$$

where w^* are extended $H^1(\Omega)$ function satisfying $w^*|_{\Gamma_D}=f_{n+1/2}$. We note that the trial function space is time-stage dependent owing to time-dependent trace data on Γ_D, while the test function space is time-stage invariant.

As usual, multiplying the converted partial differential equation by a test function Q and integrating by parts over the domain Ω, we arrive at a sequence of N abstract variational problems: Given $T_n\in\tilde{V}(\Omega)$, find $T_{n+1}\in\tilde{V}(\Omega)$ such that

$$\left.\begin{aligned} &a(T_{n+1},\ \Xi)=l(\Xi),\ \forall\Xi\in V(\Omega), \\ &n=0,\ 1,\ 2,\ \cdots,\ N-1 \end{aligned}\right\} \quad (5)$$

Here, $a(\cdot,\cdot):\tilde{V}(\Omega)\times V(\Omega)\rightarrow R$ is a bilinear functional and $l(\cdot):V(\Omega)\rightarrow R$ a linear functiona defined by

Copyright (C) 2003 NuriMedia Co., Ltd.

$$
\begin{aligned}
a(T_{n+1}, \Xi) &= \int_\Omega \rho c T_{n+1}\Xi d\Omega + \frac{\Delta t}{2}\int_\Omega k(\nabla T_{n+1}\cdot\nabla\Xi)\,d\Omega \\
&\quad + \frac{\Delta t}{2}\int_{\Gamma_c} h_c T_{n+1}^s \Xi d\Gamma \\
l(\Xi) &= \int_\Omega \rho c T_n \Xi d\Omega - \frac{\Delta t}{2}\int_\Omega k(\nabla T_n\cdot\nabla\Xi)\,d\Omega \\
&\quad + \Delta t\int_\Omega \dot{q}_{n+1/2}\Xi d\Omega \\
&\quad - \frac{\Delta t}{2}\int_{\Gamma_c} h_c(T_n^s - 2T_\infty)\Xi d\Gamma
\end{aligned}
\tag{6}
$$

where $\dot{q}_{n+1/2}$ denotes the time derivative of $q_{n+1/2}$.

The variational problem (5) has a unique solution T_{n+1} which depends continuously on the data as follows (c_1, c_2 and c_3 are positive constants) (Oden and Demkowicz 1996):

$$
\| T_{n+1}\|_{1,\Omega} \le c_1 \| \dot{q}_{n+1/2}\|_{1,\Omega} + c_2 \|(T_n^s - 2T_\infty)\|_{L^2(\Gamma_c)} + c_3 \|\{w^*\}_{n+1}\|_{1,\Omega} \tag{7}
$$

where $\|\cdot\|_{1,\Omega}$ is a first-order Sobolev norm defined by

$$
\|\Xi\|_{1,\Omega} = \left\{ \int_\Omega \{|\Xi|^2 + |\nabla\Xi|^2\}\,d\Omega \right\}^{1/2} \tag{8}
$$

2.2 Finite element approximation

For finite element approximation of the variational problem (5), we make partition Ω into a finite collection of $\aleph(\aleph^e)$ finite elements Ω_K with boundaries $\partial\Omega_K$ such that

$$
\bar{\Omega} = \bigcup_{K=1}^{\aleph^e} \bar{\Omega}_K, \quad \Omega_K \cap \Omega_L = \emptyset \ \text{ if } K \neq L \tag{9}
$$

and the finite element approximation space $V^h(\Omega)$ and $\{w^*\}_{n+1}^h$ defined by

$$
\left.
\begin{aligned}
V^h(\Omega) &= V(\Omega) \cap \prod_{K=1}^{\aleph^e} C^0(\bar{\Omega}_K) \\
\{w^*\}_{n+1}^h &= \{w^*\}_{n+1} \cap \prod_{K=1}^{\aleph^e} C^0(\bar{\Omega}_K)
\end{aligned}
\right\} \tag{10}
$$

Then, we get the following set of full-discrete finite element approximations for each time stage t_{n+1}: Given $T_n^h \in V_n^h(\Omega) + \{w^*\}_n^h$, find $T_{n+1}^h \in \{V_{n+1}^h(\Omega) + \{w^*\}_{n+1}^h\}$ such that

$$
\begin{aligned}
&a(T_{n+1}^h, \Xi^h) = l(\Xi^h), \ \forall \Xi^h \in V^h(\Omega), \\
&n = 0, 1, 2, \cdots, N-1
\end{aligned}
\tag{11}
$$

To express the above finite element approximation (11) in a usual matrix form, let us span the finite element approximation space $V^h(\Omega)$ by the finite element basis functions $\{\phi_i(\boldsymbol{x})\}_{i=1}^N$,

$$
T_{n+1}^h = \sum_{i=1}^N \bar{T}_{i,n+1}^h \phi_i(\boldsymbol{x}), \quad \Xi^h = \sum_{i=1}^n \bar{\Xi}_i^h \phi_i(\boldsymbol{x}) \tag{12}
$$

Substituting Eq. (12) into Eq. (11), we have the next successive matrix system of simultaneous linear equations, the well-known Crank-Nicolson-Galerkin scheme:

$$
\left[\boldsymbol{C} + \frac{\Delta t}{2}\boldsymbol{K}\right]\bar{\boldsymbol{T}}_{n+1}^h = \left[\boldsymbol{C} - \frac{\Delta t}{2}\boldsymbol{K}\right]\bar{\boldsymbol{T}}_n^h + \boldsymbol{F}_{n+1/2} \tag{13}
$$

Here, time-stage invariant (assuming temperature-independent material constants) matrices $\boldsymbol{C}$, $\boldsymbol{K}$ and time-stage dependent vector $\boldsymbol{F}_{n+1/2}$ are respectively expressed by

$$
\left.
\begin{aligned}
[C]_{ij} &= \int_\Omega \rho c \phi_i(\boldsymbol{x})\phi_j(\boldsymbol{x})\,d\Omega \\
[K]_{ij} &= \int_\Omega k(\nabla\phi_i(\boldsymbol{x})\cdot\nabla\phi_j(\boldsymbol{x}))\,d\Omega + \int_{\Gamma_c} h_c\phi_i(\boldsymbol{x})\phi_j(\boldsymbol{x})\,d\Gamma \\
\{F_{n+1/2}\}_i &= \Delta t\int_\Omega \dot{q}_{n+1/2}\phi_i(\boldsymbol{x})\,d\Omega - \frac{\Delta t}{2}\int_{\Gamma_c} h_c\{T_n^s - 2T_\infty\}\phi_i(\boldsymbol{x})\,d\Gamma
\end{aligned}
\right\} \tag{14}
$$

3. Stability and Convergence

Let $T(\boldsymbol{x};t)$ be an exact solution of the initial-boundary value problem (1), and denote corresponding solutions of the semi-discrete problem (2) and the full-discrete problem (11) by $T^\tau(\boldsymbol{x};t)$ and $T^h(\boldsymbol{x};t)$. In addition, we define the energy norm $\|\cdot\|_{E(\Omega)}$ by

$$
\|\cdot\|_{E(\Omega)}^{def} = a(\cdot,\cdot)^{1/2} \tag{15}
$$

Then, the total approximation error $E_T(\boldsymbol{x};t^*) = T(\boldsymbol{x};t^*) - T^h(\boldsymbol{x};t^*)$ is composed of the temporal discretization error $E_\tau(\boldsymbol{x};t^*) = T(\boldsymbol{x};t^*) - T^\tau(\boldsymbol{x};t^*)$ and the spatial approximation error $E_h(\boldsymbol{x};t^*) = T^\tau(\boldsymbol{x};t^*) - T^h(\boldsymbol{x};t^*)$ such that

$$
\begin{aligned}
E_T &= T(\boldsymbol{x};t^*) - T^h(\boldsymbol{x};t^*) \\
&= T(\boldsymbol{x};t^*) - T^\tau(\boldsymbol{x};t^*) + T^\tau(\boldsymbol{x};t^*) - T^h(\boldsymbol{x};t^*) \\
&= E_\tau + E_h
\end{aligned}
\tag{16}
$$

with the inequality:

$$
\begin{aligned}
\|E_T\|_{E(\Omega)} &= \|E_\tau + E_h\|_{E(\Omega)} \\
&\le \|E_\tau\|_{E(\Omega)} + \|E_h\|_{E(\Omega)}
\end{aligned}
\tag{17}
$$

Now, let us denote the operator $\nabla\cdot(-k\nabla)$ by A, and define the subspace $D(A)$ of $L^2(\Omega)$ such as

$$
\left.
\begin{aligned}
D(A) &= \{T \in H^2(\Omega) : T = 0 \text{ on } \Gamma_D\} \\
A &: L^2(\Omega) \supset D(A) \to L^2(\Omega)
\end{aligned}
\right\} \tag{18}
$$

Copyright (C) 2003 NuriMedia Co., Ltd.

then, the operator A becomes self-adjoint. From the spectral decomposition theorem, we have (see Oden and Demkowicz (1996) for details on the both)

$$AT(\boldsymbol{x};t)=\int_{-\infty}^{\infty}\lambda dI(\lambda)\,T(\boldsymbol{x};t),\quad \forall T(\boldsymbol{x};t)\in D(A) \tag{19}$$

where λ is an eigenvalue distribution and $I(\lambda)$ defined as the spectral family of the operator A. Moreover, a unique weak solution is expressed by

$$\begin{aligned}T(\boldsymbol{x};t)&=e^{-(At/\rho c)}T_0(\boldsymbol{x})\\&=\int_{-\infty}^{\infty}e^{-(\lambda t/\rho c)}dI(\lambda)\,T_0(\boldsymbol{x})\end{aligned} \tag{20}$$

with the conserved energy:

$$\begin{aligned}\|T(\boldsymbol{x};t)\|^2&=\int_{-\infty}^{\infty}|e^{-(\lambda t/\rho c)}|^2 d(I(\lambda)\,T_0,\,T_0)\\&=\|T_0(\boldsymbol{x})\|^2,\ \forall t\geq 0\end{aligned} \tag{21}$$

In which, $(\cdot,\cdot)$ denotes the inner product.

From the operator A, the spectral decomposition and the Trace theorem, we can define the energy norm as follows ($\forall T\in D(A)$):

$$\begin{aligned}&\|T(\boldsymbol{x};t)\|^2_{E(\Omega)}\\&\stackrel{\text{def}}{=}\int_{\Omega}\left\{|T|^2+\frac{kt}{2\rho c}|\nabla T|^2\right\}d\Omega+\int_{\Gamma_c}\frac{h_c t}{2\rho c}|T|^2 d\Gamma\\&\leq C_1(h_c/\kappa)\int_{-\infty}^{\infty}|e^{-(\lambda t/\rho c)}|^2(1-\lambda t/2\rho c)\,d(I(\lambda)\,T_0,\,T_0)\end{aligned} \tag{22}$$

Theorem 3.1 The Crank-Nicolson-Galerkin scheme (13) exhibits the following stable convergent error bound

$$\begin{aligned}&\|E_T\|_{E(\Omega)}\leq C(h_c/\kappa)\,t^*\\&\left\{(\Delta t)^2\|A^3[T_0(\boldsymbol{x})/(\rho c)^3]\|_{E(\Omega)}+\frac{h^{\mu-1}}{\sigma}\|T_0(\boldsymbol{x})\|_{H^\mu(\Omega)}\right\}\end{aligned} \tag{23}$$

where $\sigma=(\Delta t/h)$ and $\mu=\min(s-1,\,p)$, while denoting s and p as the regularity of $T_0(\boldsymbol{x})$ and the order of approximation polynomials (see Appendix for the proof).

Even though the Crank-Nicolson-Galerkin scheme is unconditionally convergent, it may lead to oscillatory results unless the time-step size is elaborately chosen. This oscillation tendency is proportional to the intensity of sudden change in the temperature time-history response by impulsive thermal load or/and abrupt change in the boundary condition. One crucial situation in heat transfer problems becomes a thermal shock problem.

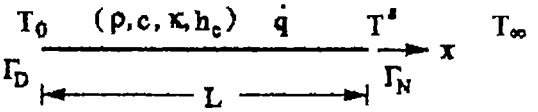

Fig. 2 An one-dimensional heat convection problem

Since the time-history singularity is closely related to the dominant eigenmode of the free system response, it is general to examine finite-element eigenvalues. Eigenvalues of the free temperature response of the two-dimensional problem (1) are given by

$$\lambda_{mn}=(\pi^2\kappa/\rho c)[(m/L_x)^2+(n/L_y)^2],\quad m,\,n=1,\,2,\,\cdots \tag{24}$$

where L_x and L_y are characteristic lengths of the problem domain $\Omega\in R^N$ ($N=2$). Letting $\delta_{\min}$ be a shortest relative distance between two adjacent finite-element nodes, the largest eigenvalue (i.e. corresponding to the shortest wavelength) becomes $\lambda_{\max}\approx N[\pi/\delta_{\min}]^2(\kappa/\rho c)$.

In order to prevent the oscillation due to the fundamental eigenmode, it has been suggested that one should select the critical time-step size satisfying (C_c of 2~3 (Burnett 1988))

$$(\Delta t)_{crit}\approx 2C_c/\lambda_{\max} \tag{25}$$

4. Numerical Experiments

Figure 2 depicts an one-dimensional heat convection model, where the left end is kept to initial temperature T_0 while the right end is exposed to the surrounding with constant temperature T_∞. The numerical data taken for our experiments are contained in Table 1.

In order to examine the oscillation behavior in the time-history response of temperature, we first carried out the preliminary simulation for three different uniform time steps, 3, 1 and 0.1 sec with a uniform finite element mesh constructed with eight quadratic elements. We observed that the case with time step of 0.1 sec does not produce

Copyright (C) 2003 NuriMedia Co., Ltd.

Table 1 Geometry and material data for numerical experiments

Material parameters		Simulation parameters	
Density, ρ(kg/m^3)	5	Length, L(m)	1
Specific heat, c(J/kg·K)	2	Time interval, t^*(sec)	15
Thermal conductivity, κ(W/m·K)	1	Initial temperature, $T_0(K)$	300
Convection coefficient, h_c(W/m^2·K)	5	Surrounding temperature, T_∞(K)	300
Heat generation, $\dot{q}$(W/m^3)	10^4		

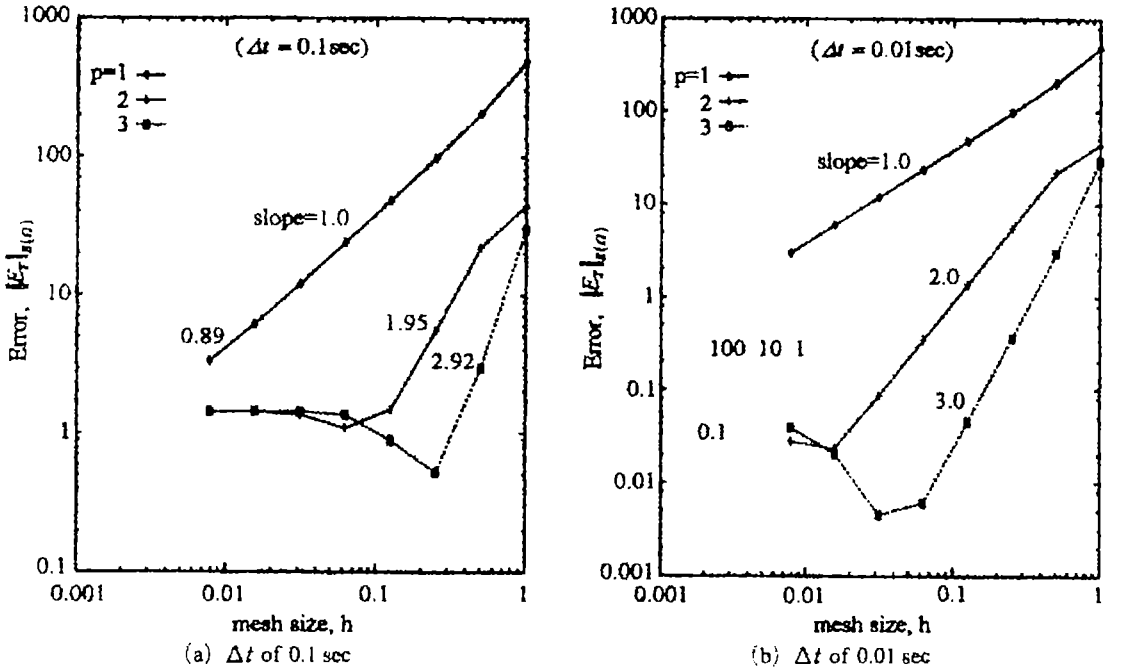

Fig. 3 The h-convergence rates at t of 1.0 sec

any remarkable oscillation phenomenon, from the time-history response plot. Calculating the criti-cal time step $(\Delta t)_{cri}$ according to the above-mentioned theoretical formula (25), we have 0.016 sec (with C_c of 2). Even though a considerably larger time step compared to $(\Delta t)_{cri}$ seems to lead to the acceptable numerical results, we will see that such a choice can not secure optimal h- and p-convergence rates in the region where the oscillation error dominates in the total error.

Next four Figs. 3(a)-4(b) represent numerical results of the parametric dependence of the time-step size on the h-convergence rate for different mesh parameters h of 1, 1/2, 1/4, 1/16, 1/32, 1/64 and 1/128 and of 1, 2 and 3. We note here that the mesh size refers to the relative finite-element length to the total length L, and which implies $\delta_{min}=h/p$. The errors are calculated at time t of 1.0 sec, according to the energy-norm defined in Eq. (22). As a reference temperature field, we approximate the exact solution using the time step of sec and the fine finite-element mesh constructed with two hundreds uniform 9th order elements.

According to Theorem 3.1, the optimal h-convergence rate is proportional to $\mu=\min(s-1, p)$ when the regular partitioning parameter σ is not enforced. On the other hand, from Eq. (25), the critical time-step size is in inverse proportion to the shortest relative distance δ_{min}. From Fig. 3(a), we see the remarkable deterioration in the h-

Copyright (C) 2003 NuriMedia Co., Ltd.

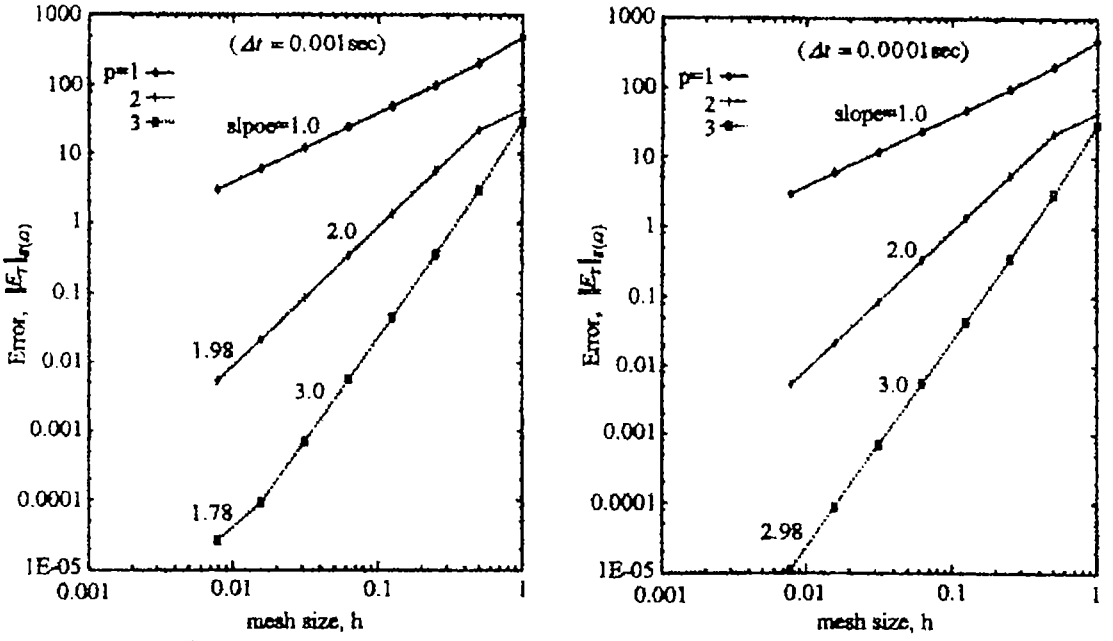

(a) Δt of 0.001 sec (b) Δt of 1×10^{-4} sec

Fig. 4 The h-convergence rates at t of 1.0 sec

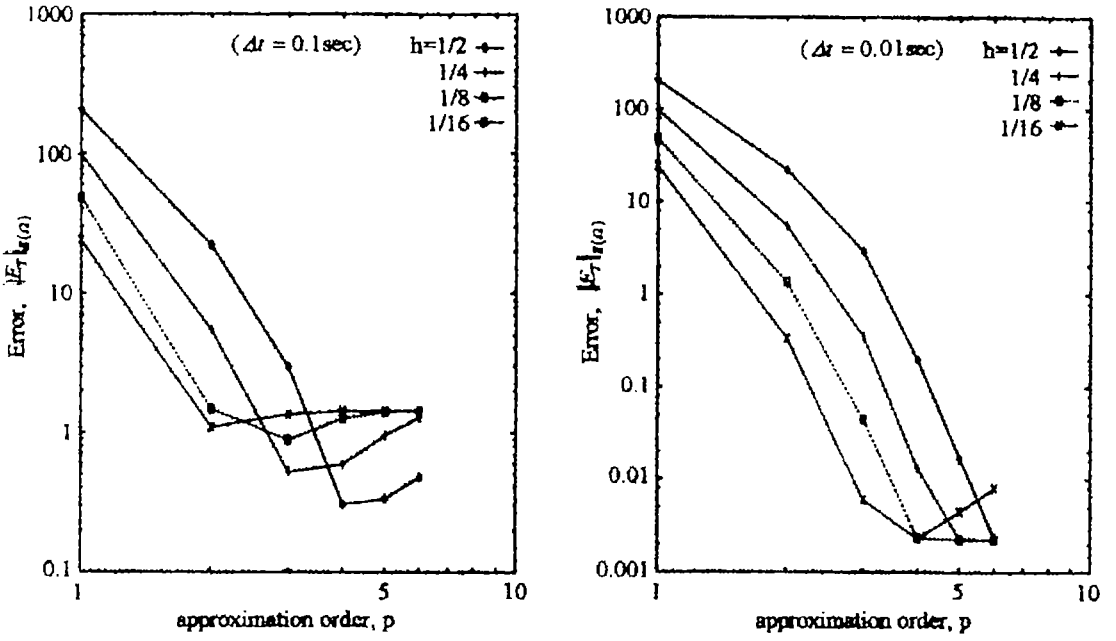

(a) Δt of 0.1 sec (b) Δt of 0.01 sec

Fig. 5 The p-convergence rates at t of 1.0 sec

convergence rate owing to the insufficiently small time step for fine meshes beyond h of 1/64 for linear, 1/8 for quadratic and 1/4 for cubic elements, respectively. However, as shown in the other three figures, the relative distances showing optimal h-convergence rates becomes shorter as

Copyright (C) 2003 NuriMedia Co., Ltd.

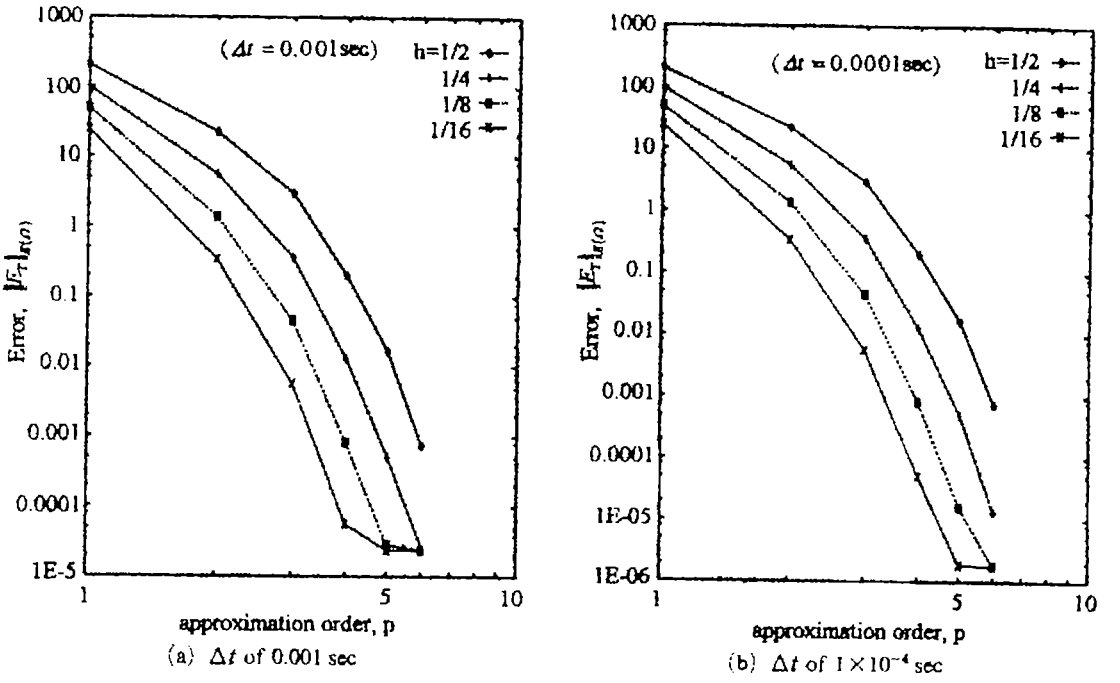

Fig. 6 The p-convergence rates at t of 1.0 sec

the time step decreases. From the plots in Figs. 3(b)-4(b), linear, quadratic and cubic elements show optimal h-convergence rates up to h of 1/128 when the time step is less that 0.01, 0.001 and 1×10^{-4} sec, respectively.

Numerical results associated with the parametric investigation on the p-convergence rate to the time-step size for four different mesh sizes are represented in Figs. 5(a)-6(b). We first see, from Fig. 5(a), that the considerable deterioration in the p-convergence rates suffering from the insufficiently small time step. The prevalence of such a deterioration increases in proportion to the inverse of the mesh size, and which is consistent with the above-mentioned analytical results.

However, we see the improvement in the p-convergence rate for each mesh size according to the time-step decrease, from Figs. 5(b)-6(b). The case of $h=1/2$ recovers the optimal p-convergence rate up to p of 6 when the time step is less than 0.01 sec while the cases of $h=1/4$ and 1/8 for the time steps less than 0.001 and 1×10^{-4} sec, respectively. But, the finest case does not show the optimal p-convergence rate even when the time step is reduced to 1×10^{-4} sec, as presented in Fig. 6(b).

Figure 7(a) shows the variations of the total error measured at time $t=1.0$ sec along the time-step size for different mesh sizes. Recalling that the total error is contributed by the time discretization and the finite element approximation, we obviously observe each contribution from the plots. For each mesh size, the error level corresponding to the saturated horizontal line indicates the error portion by the finite element approximation, while the difference in error levels between the saturated and the inclined locations corresponds to the error portion by the insufficiently small time step. We further see that the time step securing the optimal h-convergence rate becomes continuously smaller as the finite-element mesh is getting refined.

The relation between the time-step size securing optimal h- and p-convergence rate and the degree of freedom is presented in Fig. 7(b). The linear dependence of the time-step on the degree of freedom implies to the enforcement of the regular time-space partition introduced in Eq. (A6). It is worth to mention that the h-convergence rate is reduced by one order when the time

Copyright (C) 2003 NuriMedia Co., Ltd.

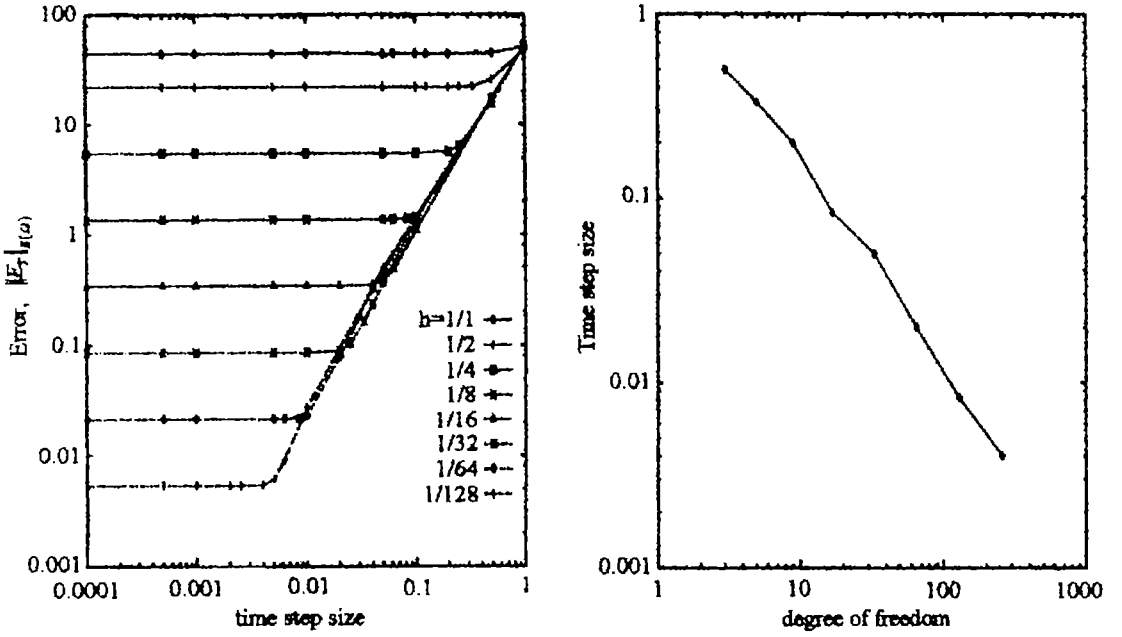

(a) Influence of Δt and h on $\| E_T \|_{E(a)}(p=2)$ (b) Relation between Δt and DOF

Fig. 7 Parametric conditions for securing optimal h- and p-convergence rates

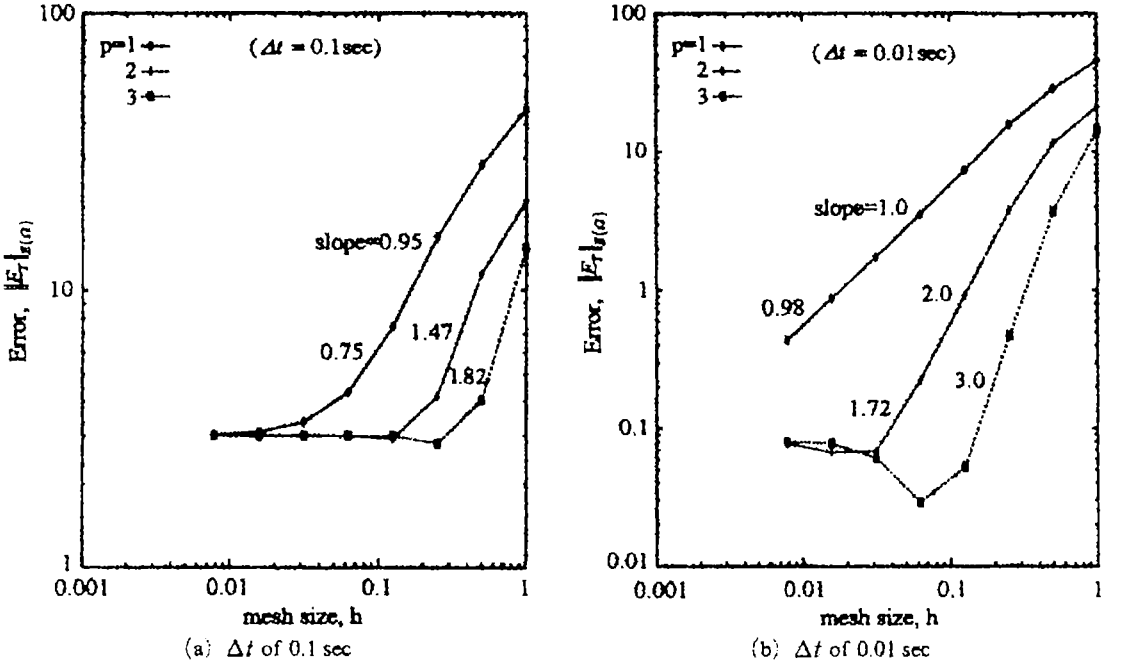

(a) Δt of 0.1 sec (b) Δt of 0.01 sec

Fig. 8 The h-convergence rates at t of 0.1 sec

step is regularly reduced together with the mesh refinement, as declared in Theorem 3.1.

In order to examine the difference in the h- and p-convergence rates owing to the difference in temperature time-history response singularity, we next measure the total error at t of 0.1 sec and

Copyright (C) 2003 NuriMedia Co., Ltd.

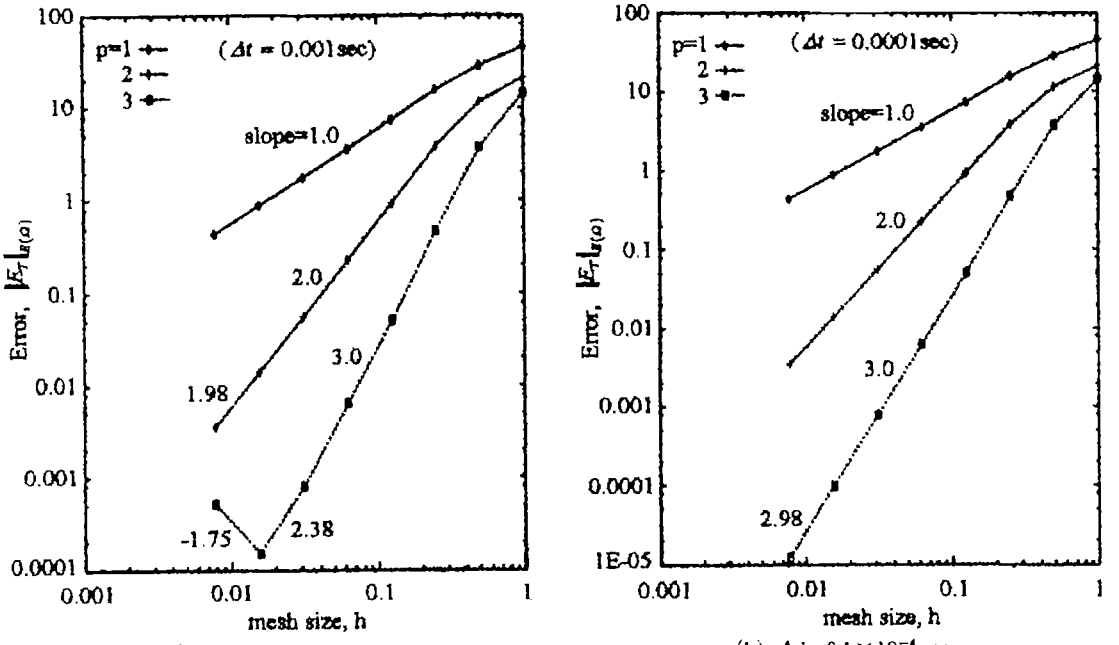

(a) Δt of 0.001 sec (b) Δt of 1×10^{-4} sec

Fig. 9 The h-convergence rates at t of 0.1 sec

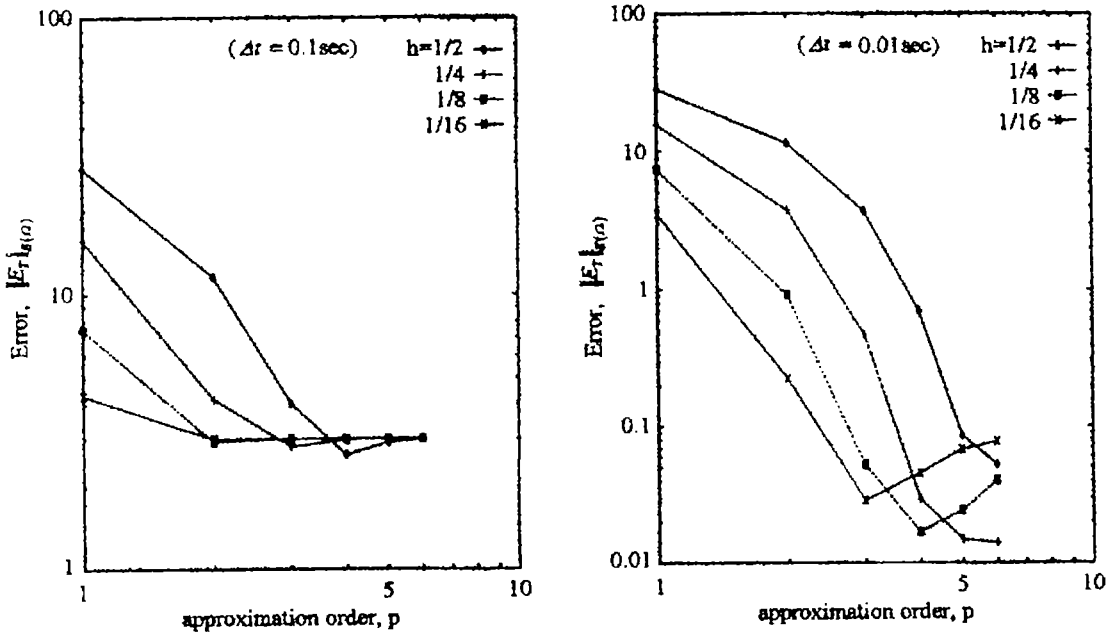

(a) Δt of 0.1 sec (b) Δt of 0.01 sec

Fig. 10 The p-convergence rates at t of 0.1 sec

compute the corresponding h- and p-convergence rates. The estimated h- and p-convergence rates are presented in Figs. 8(a)-9(b) and Figs. 10(a)-11(b), respectively. By comparing Figs. 8(a) and 10(a) to Figs. 3(a) and 5(a) showing the h- and p-convergence rates for Δt of 0.1 sec, we

Copyright (C) 2003 NuriMedia Co., Ltd.

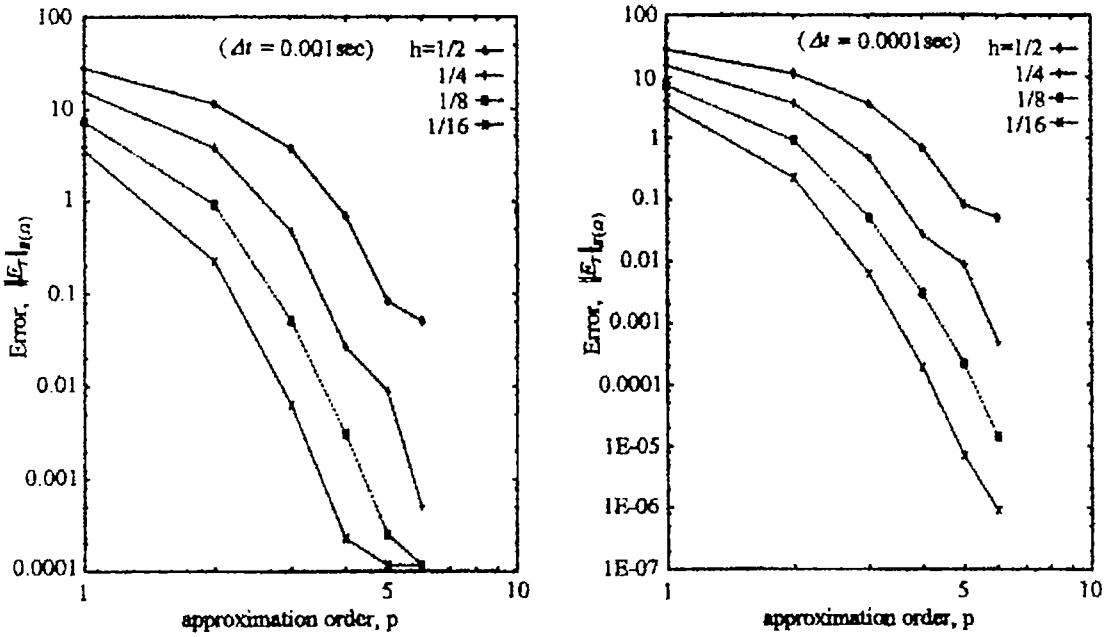

(a) Δt of 0.001 sec (b) Δt of 1×10^{-4} sec

Fig. 11 The p-convergence rates at t of 0.1 sec

see the more serious deterioration in the optimal convergence when t is 0.1 sec. However, by comparing both of the remaining figures for $\Delta t \geq 0.01$ sec, we observe that this tendency owing to the singularity increase in the transient region becomes smaller as the time-step size becomes smaller. This is because, for a given finite-element mesh, an insufficiently small time-step size for the case of $t=0.1$ sec requiring smaller time-step size compared to the case of $t=1.0$ sec leads to more critical situation.

5. Conclusions

In this paper, we first presented the derivation of a priori error estimate, for the Crank-Nicolson-Galerkin scheme for convection-type heat transfer problems, which reflects the time-discretization and the finite-element approximation errors. According to the derived error estimate, the h- and p-convergence rates lose their optimal convergence rates by one when the regular time-space partition is enforced. From the numerical results obtained from the one-dimensional model problem, we observed that the time-step size securing optimal h- and p-convergence is in linear relation to the DOF.

In addition, we carried out the parametric numerical simulation to investigate the effect of the time-step size on the h- and p-convergence rates when the regular time-space partitioning condition is not enforced. We observed that the optimal h- and p-convergence rates are strongly influenced by h and p so that the optimal convergence rates are secured only when the total error is not affected by the oscillation behavior. On the other hand, we compared the numerical errors measured at two different time stages, t of 0.1 and 1.0 sec, in order to examine the effect of the time-history singularity. For the same time-step size, we observed more serious deterioration in optimal convergence rates at t of 0.1 sec, and which is owing to singularity increase in the temperature time-history response.

Acknowledgment

This work was supported by grant No. R01-2001-00383 from the Korea Science & Engineering Foundation.

Copyright (C) 2003 NuriMedia Co., Ltd.

References

Bieniasz, L. K., Osterby, O. and Britz, D., 1997, "The Effect of the Discretization of the Mixed Boundary Conditions on the Numerical Stability of the Crank-Nicolson Algorithm of Electrochemical Kinetic Simulations," *Computers Chem.*, Vol. 21, No. 6, pp. 391~401.

Burnett, D. S., 1988, *Finite Element Analysis : From Concepts to Applications*, Addison Wiley.

Cho, J. R. and Oden, J. T., 2000, "Functionally Graded Material : a Parametric Study on Thermal Stress Characteristics Using the Crank-Nicolson-Galerkin Scheme," *Comput. Methods Appl. Mech. Engrg.*, Vol. 188, pp. 17~38.

Comini, G. and Manzan, M., 1994, "Stability Characteristics of Time Integration Schemes for Finite Element Solutions of Conduction-Type Problems," *Int. J. Numer. Methods Heat Fluid Flow*, Vol. 4, pp. 131~142.

Johnson, C., 1987, *Numerical Solution of Partial Differential Equations by the Finite Element Method*, Cambridge University Press, New York.

Morjaria, M. and Mukherjee, S., 1981, "Finite Element Analysis of Time-Dependent Inelastic Deformation in the Presence of Transient Thermal Stresses," *Int. J. Numer. Methods Engrg.*, Vol. 17, pp. 909~921.

Oden, J. T. and Demkowicz, L. F., 1996, *Applied Functional Analysis*, CRC Press, New York.

Renaut, R., 1997, "Stability of a Chebychev Pseudospectral Solution of the Wave Equation with Absorbing Boundaries," *Comput. Appl. Math.*, Vol. 87, pp. 243~259.

Suresh, S., Giannakopolos, A. E. and Olsson, M., 1994, "Elastic Analysis of Thermal Cycling : Layered Materials with Sharp Interfaces," *J. Mech. Phys. Solids*, Vol. 42, No. 6, pp. 979~1018.

Tsukerman, I., 1995, "A Stability Paradox for Time-Stepping Scheme in Coupled Field-Circuit Problems," *IEEE Trans. Magn.*, Vol. 31, No. 3, pp. 1857~1860.

Ciarlet, P. G., 1987, *The Finite Element Methods for Elliptic Problems*, North-Holland, New York.

Appendix

We first derive a priori temporal error estimation. For any time stage, the transient (or amplitude) operator R is represented by a rational function of the operator A

$$\begin{aligned} T_{n+1}^I(\boldsymbol{x}) &= R\,T_n^I(\boldsymbol{x}) \\ &= \sum_{i=0}^{\infty} r(\lambda_i \Delta t/\rho c)\{\alpha_i \boldsymbol{e}_i\} \\ &= r(A\Delta t/\rho c)\,T_n^I(\boldsymbol{x}) \end{aligned} \tag{A1}$$

and furthermore

$$T_{n+1}^h(\boldsymbol{x}) = R_h T_n^h(\boldsymbol{x}) \tag{A2}$$

From the weak solution of initial-boundary value problem (1), it is obvious that $T_{n+1}(\boldsymbol{x}) = e^{-(A\Delta t/\rho c)} T_n(\boldsymbol{x})$. Then, the temporal discretization error for a single time-step Δt is bounded by

$$\begin{aligned} \|E_t^n\|_{E(\Omega)} &= \|T_{n+1}(\boldsymbol{x}) - T_{n+1}^I(\boldsymbol{x})\|_{E(\Omega)} \\ &= \|e^{-(A\Delta t/\rho c)} T_n(\boldsymbol{x}) - r(A\Delta t/\rho c)\,T_n(\boldsymbol{x})\|_{E(\Omega)} \\ &\le C_1(h_c/\kappa)\int_{-\infty}^{\infty} |e^{-(\lambda\Delta t/\rho c)} - r(A\Delta t/\rho c)|^2 \\ &\quad (1-\lambda\Delta t/2\rho c)\, d(I(\lambda)\,T_n,\ T_n) \\ &\le C_2(h_c/\kappa)(\Delta t)^3 \int_{-\infty}^{\infty} |\lambda^3|^2 (1-\lambda\Delta t/2\rho c) \\ &\quad d(I(\lambda)\,T_n/(\rho c)^3,\ T_n/(\rho c)^3) \\ &= C_2(h_c/\kappa)(\Delta t)^3 \|A^3[T_n/(\rho c)^3]\|_{E(\Omega)} \end{aligned} \tag{A3}$$

Then, the entire temporal discretization error of the semi-discrete problem (2) starting form $T_0(\boldsymbol{x})$ is

$$\begin{aligned} \|E_t\|_{E(\Omega)} &= \|T_N(\boldsymbol{x}) - T_N^I(\boldsymbol{x})\|_{E(\Omega)} \\ &= \|e^{-(A\Delta t/\rho c)} T_0(\boldsymbol{x}) - r^N(A\Delta t/\rho c)\,T_0(\boldsymbol{x})\|_{E(\Omega)} \\ &\le N\|e^{-(A\Delta t/\rho c)} T_0(\boldsymbol{x}) - r(A\Delta t/\rho c)\,T_0(\boldsymbol{x})\|_{E(\Omega)} \\ &\le C_2(h_c/\kappa)(\Delta t)^2 (N\Delta t)\|A^3[T_0(\boldsymbol{x})/(\rho c)^3]\|_{E(\Omega)} \\ &= C_2(h_c/\kappa)\, t^*(\Delta t)^2 \|A^3[T_0(\boldsymbol{x})/(\rho c)^3]\|_{E(\Omega)} \end{aligned} \tag{A4}$$

Next, for a derivation of a priori spatial error estimation, let us define the orthogonal projection operator $\prod_h$ and a positive constant σ such that

$$\prod_h : V(\Omega) \to V^h(\Omega),\ \prod_h T = T^h \tag{A5}$$

$$\sigma = \Delta t/h \tag{A6}$$

where σ enforces a regular partitioning of time-space domain. Then, the spatial error in the energy norm is derived according to

Copyright (C) 2003 NuriMedia Co., Ltd.

$$\begin{aligned}\| E_h \|_{E(\Omega)} &= \| T_N^h(x) - T_N^h(x) \|_{E(\Omega)} \\ &= \| R^N T_0(x) - R_h^N \prod_h T(x) \|_{E(\Omega)} \\ &\le \sum_{i=0}^{N-1} \| R T_i(x) - R_h T_i(x) \|_{E(\Omega)} \\ &\le N \| R - R_h \|_{E(\Omega)} \| T_0(x) - \prod_h T_0(x) \|_{E(\Omega)} \\ &\le N(\| R \|_{E(\Omega)} + \| R_h \|_{E(\Omega)}) \| T_0(x) - \prod_h T_0(x) \|_{E(\Omega)}\end{aligned} \tag{A7}$$

Here, the error bound $\| T(x) - \prod_h T(x) \|_{E(\Omega)}$ for quasi-uniform finite element space follows from the well-known standard error bound (see Ciarlet (1987) for more details)

$$\begin{aligned}&\| T_0(x) - \prod_h T_0(x) \|_{E(\Omega)} \\ &\le \inf_{T_0^h \in V^h(\Omega)} (\| T_0(x) - T_0^h(x) \|_{E(\Omega)}) \\ &\le C_3 (h_c/\kappa) \max_{x \in \Omega} \left\{ 1, \frac{\Delta t}{2\rho c/\kappa} \right\} h^\mu \| T_0(x) \|_{H^\mu(\Omega)} \\ &= C_3 (h_c/\kappa) h^\mu \| T_0(x) \|_{H^\mu(\Omega)}\end{aligned} \tag{A8}$$

where $\mu = \min(s-1, p)$ with s, p denoted as the regularity of $T_0(x)$ and the order of approximation polynomials, respectively. We now consider the error bounds of the two transient operators R and R^h in Eq. (A7). First, from the fact that $r(A\Delta t/\rho c)$ is a contraction in the energy norm, we have

$$\begin{aligned}\| R \|_{E(\Omega)} &= \sup_{T_i (T \neq 0)} \frac{\| RT \|_{E(\Omega)}}{\| T \|_{E(\Omega)}} \\ &= \sup_{T_i (T \neq 0)} \frac{\| r(A\Delta t/\rho c) \|_{E(\Omega)} \| T \|_{E(\Omega)}}{\| T \|_{E(\Omega)}} \le 1\end{aligned} \tag{A9}$$

Next, from the stability analysis, we have

$$\| R_h \|_{E(\Omega)} = \sup_{T^h, (T^h \neq 0)} \frac{\| R_h T^h \|_{E(\Omega)}}{\| T^h \|_{E(\Omega)}} < 1 \tag{A10}$$

Substituting Eqs. (A8)-(A10) into Eq. (A7), we arrive at a priori spatial error estimation :

$$\begin{aligned}\| E_h \|_{E(\Omega)} &\le 2 C_3 (h_c/\kappa) N h^\mu \| T_0(x) \|_{H^\mu(\Omega)} \\ &= (2 C_3 (h_c/\kappa) t^*/\sigma) h^{\mu-1} \| T_0(x) \|_{H^\mu(\Omega)}\end{aligned} \tag{A11}$$

Combining the temporal and spatial error estimations Eqs. (A4) and (A11), we finally obtain a priori total error estimate, for the Crank-Nicolson-Galerkin scheme with regular partitioning of time-space domain :

$$\begin{aligned}\| E_T \|_{E\Omega} &= \| E_t \|_{E\Omega} + \| E_h \|_{E\Omega} \\ &\le C \{ (h_c/\kappa) t^* \{ (\Delta t)^2 \| A^{\frac{1}{2}} T_0(x, (\rho c)^{\frac{1}{2}} \|_{E\Omega} + \frac{K^2}{\sigma} \| T_0(x) \|_{H^\mu \Omega} \}\end{aligned} \tag{A12}$$

Then, from the Lax equivalence theorem (Oden and Demkowicz 1996), the proof is completed.

Copyright (C) 2003 NuriMedia Co., Ltd.